

Modified Strategy for Calibration and Energy Reconstruction

Jianglai Liu, Bob McKeown
Caltech

November 16, 2006

Abstract

In this note, we outline a modified plan for calibration and event reconstruction, in response to the concerns raised at the Berkeley DoE review.

1 Introduction

Previously in [1], we explored the effectiveness of a simple calibration system with ^{68}Ge , ^{60}Co , and Cf sources. We divided the main purpose of the system into two aspects: a) to monitor the change/difference in detector conditions, and b) to calibrate detector response at the three source energies to define energy scales and cuts. For aspect a), a program was outlined in [1], which was shown capable of telling the change of various parameters, and making *relative* measurements of them. For aspect b), we proposed a simple (position independent) energy reconstruction method. It is based on a non-linear fit to the three source yields at detector center, modified by a scaling factor determined from the ratio of the uniform to center neutron yield using spallation neutron. We demonstrated that for a pair of detectors with very different parameters, if this energy reconstruction is applied consistently to both, one is still able to make the neutron and positron efficiencies of the two “identical”.

With regard to this calibration/reconstruction methodology, several comments/concerns were raised during the Berkeley review:

- One needs to establish a clear connection between aspect a) and the final sensitivity of the experiment. Put it differently, how precisely individual detector parameters need to be calibrated?
- Aspect a) needs to be refocused on making *absolute* measurements to detector parameters, including “bad” conditions such as the degradation of the bottom reflector and the dirt accumulated at the bottom of acrylic.
- The connection between aspects a) and b) in [1] is missing. The simple energy reconstruction does not take detector parameters as input, which is intellectually unsatisfying. Instead, a vertex dependent energy reconstruction, with calibrated parameters as input, is the more preferred approach.

The rest of the note is organized based on these three charges. In Sec. 2, we discuss the calibration specs on individual parameters. A detailed program is outlined in Sec. 3 to address the absolute measurements of detector parameters, and we back up our program with some proof-of-principle simulations. A few additional diagnostic devices are proposed. Then in Sec. 4, we briefly discuss the modified energy reconstruction procedure. Finally, an outline of future direction of work is given in Sec. 5.

2 Calibration “Specs” for Detector Parameters

Details of the three-zone detector module is described in Chapter 5 in [2]. In the Monte Carlo, aside from the basic 3-zone geometry, the following list of parameters “defines” a detector: the light yields in the target region (Y_{tgt}) and the gamma catcher (Y_{gcat}), the attenuation lengths of the target (L_{tgt}), gamma catcher (L_{gcat}), and mineral oil (L_{mo}), the attenuation lengths of the inner and outer acrylic ($L_{\text{acry}}^{\text{in}}$ and $L_{\text{acry}}^{\text{out}}$), the

(diffusive) reflectivity of the stainless steel tank (R_{tank}), the (specular) reflectivity of the top and bottom reflectors (R_{top} and R_{bottom}). To model the potential dirty bottom of the acrylic tank, we implemented a 1 cm layer of light-absorbing liquid at the bottom of the two vessels, with an attenuation length of $L_{\text{dirt}}^{\text{in}}$ and $L_{\text{dirt}}^{\text{out}}$ for the inner and outer vessels, respectively. For reference, the “nominal” values of these parameters are listed in Table 1.

Parameter	Nominal Value	Tolerance
Y_{tgt}	9000/MeV	$\pm 1.0\%$
Y_{gcat}	9000/MeV	$\pm 1.6\%$
L_{tgt}	9 m	$\pm 5.4\%$
L_{gcat}	10 m	$\pm 11.2\%$
L_{mo}	13 m	$\pm 15.0\%$
$L_{\text{acry}}^{\text{in}}$	5 m	> 1 m
$L_{\text{acry}}^{\text{out}}$	5 m	> 1 m
R_{tank}	0.1	$\pm 26\%$
R_{top}	0.8	$\pm 7.3\%$
R_{bottom}	0.8	$\pm 7.3\%$
$L_{\text{dirt}}^{\text{in}}$	10 cm	25%
$L_{\text{dirt}}^{\text{out}}$	10 cm	60%

Table 1: *The nominal values of detector parameters considered in this study and their specs. See text for explanations.*

The question we shall address next is “how precisely one has to know these parameters to fulfill the sensitivity requirement of the experiment?” To achieve a sensitivity of 0.01 in $\sin^2 2\theta_{13}$, the total detector-related (relative) systematic uncertainty per module has to be controlled under 0.38%, which requires that the combined uncertainty in neutron and positron detection efficiencies be $< 0.2\%$ [2]. It has been shown in [1] and [2] that the neutron efficiency is more sensitive to the change of detector parameters, and a 1% uncertainty in 6 MeV cut leads to a 0.2% uncertainty in the neutron efficiency. Therefore, the question can be naturally cast into “how much variation of a given parameter will lead to a 1% change in the 6 MeV energy scale, or 0.2% change in the neutron efficiency?”

To answer this, a set of *Geant4* simulations were carried out. In each MC run, neutrons from inverse-beta reactions were distributed uniformly inside the target region, and we perturbed a given parameter from its nominal. In the total PE spectrum, the location of the n-Gd capture peak was obtained via an asymmetric gaussian fit, and we defined the “6 MeV” cut as 3/4 of that peak then calculated the resulting neutron efficiency. Due to limited MC statistics, it is much easier to observe a 1% change in the n-Gd peak than a 0.2% change in the neutron efficiency in most cases. Therefore, the tolerance or spec for individual parameters were calculated based on the variation of the n-Gd peak. Two exceptions are the gamma catcher light yield Y_{gcat} and the dirt attenuation lengths, which we shall elaborate on a little later. To summarize, the spec values (all fractional to the nominal) are listed in the last column in Table 1 [§].

It is worth clarifying that we have made a somewhat ambiguous argument that “1% change in n-Gd peak in the PE spectrum = 1% change in 6 MeV energy scale”. The logic goes as follows. Imagine that we think a parameter is p with a true value p_{true} , and that p moves the n-Gd PE peak up by 1% in the MC relative to that for p_{true} . Then if we use p in the reconstruction (with all other parameter holding at their true values), it is going to predict a 1% too high *energy* for the n-Gd peak. Relative to this “wrong-by-1%” energy spectrum, the 6 MeV neutron cut is changed by 1% as well, which typically leads to a 0.2% change in neutron efficiency.

Let us make some further remarks. First, the nominal values in Table 1 are only some arbitrary inputs

[§]Strictly speaking, the specs on attenuation parameters should be asymmetric. However, for tight variation that we consider, the upper and lower specs are approximately the same.

to the simulation. **The spec there should be interpreted as the precision to which one needs to calibrate a given parameter, rather than an absolute tolerance from the nominal that one has to build the detectors.** For a near and far detectors pair, the actual values for any given parameter can both be fairly different from the nominal, as long as they can be *calibrated* to the specified precision. Second, for parameters related to the light absorption, the constraint can be different depending on the actual value. For example, we have very conservatively chosen 10 cm attenuation length to model the dirt. Were the attenuation length of the “dirt” 10 m, it would be safe to simply ignore its existence. Third, varying each parameter within spec according to Table 1 would change either the 6 MeV scale by 1% or neutron efficiency by 0.2%, and we have 12 of these parameters! Before we get too distressed, we should keep the following points in mind: A) Most detector parameters will be measured very accurately before they get deployed underground. During the course of the experiment, we shall be focusing on measuring the changes relative to the initial values in situ, which is less difficult than an absolute measurement without reference value. B) Within a near/far pair of detectors, the initial conditions will be made as identical as possible. It is fair to derive our spec by assuming that only one of these changes in a significant manner later in time. C) With the constraints set by the source calibration, systematic uncertainties of individual parameters are likely to be correlated in such a way to keep the resulting energy spectrum intact. For instance, a “too high” light yield is likely to be accompanied by a “too low” attenuation length, so there is a net cancellation of effects. For these reasons, we shall be more optimistic that a good calibration program can achieve the challenging goal of the experiment. Fourth, as mentioned earlier, in studying the role of the gamma catcher light yield Y_{gcat} or the dirt attenuation, we realized that the rule of “1% n-Gd peak change \iff 0.2% neutrons efficiency” breaks down. In Fig. 1, the delayed energy spectrum for $Y_{\text{gcat}}=6000$ and $12000/\text{MeV}$ (with a common $Y_{\text{tgt}}=9000/\text{MeV}$) are overlaid. Among the three, the n-Gd peaks varied very little ($<1\%$), whereas the neutron efficiency varied from 86.4% (6000/MeV) to 94.0% (12000/MeV). This can be understood from the fact that the pronounced n-Gd peaks are made by events from the inner region of the target, which deposit their energy solely inside the target. Thus the peak location is very much defined by Y_{tgt} . On the other hand, events close to the edge of the fiducial (which leak energy into the gamma catcher and mineral oil) contribute to the low energy tails. Different Y_{gcat} affects relative position of the tail to the peak, which in turn affects the neutron efficiency in a significant way. The impact of the dirty acrylic to the neutron efficiency is similar: for different dirt attenuation, the “visibility” of the photon energy deposited at the bottom of the target or gamma catcher will be different, which alters the low energy tail significantly.

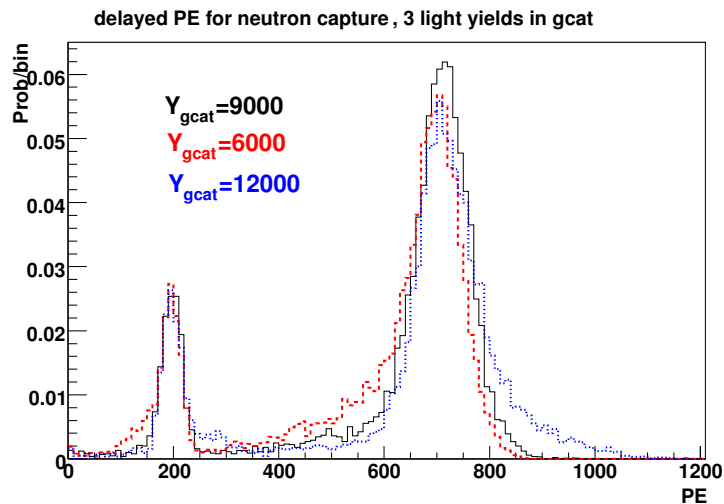


Figure 1: *Neutron capture PE spectra for three different light yields in the gamma catcher: [black=9000, red dashed=6000, blue dotted=12000/MeV]. The light yield for the target is kept at 9000/MeV for all three histograms.*

3 Calibration Program for Individual Detector Parameters

In this section, we will outline a detailed program to make absolute calibrations of individual detector parameters.

3.1 PMT Timing, Gain, Threshold, and Relative Quantum Efficiency

An LED system with a control trigger can be used to calibrate the PMT timing. Due to the cylindrical shape of the detector, we proposal to move the LED diffuser ball along the central z axis, and calibrate the PMT timing ring by ring. At the same time, the absolute gain of the PMTs can be calibrated by the ADC peaks of the single photoelectrons, after which individual discriminator thresholds can be set.

Assuming a perfect azimuthal symmetry, the relative quantum efficiencies for different tubes in the same ring can be calibrated based on the measured rate during the LED z scan. A tight timing cut might be necessary to remove the background counts as well as photons reflected from the wall. It is reasonable to expect that the average QEs for different rings are very similar. One can combine the solid angle information with the measured rates to further constrain them. In principle, only a global factor in QE will be left undetermined after this step for all the tubes in a detector module.

We envision that an LED z scan will happen during the commissioning stage, and perhaps on a monthly or quarterly basis afterwards. 100 single photoelectrons render a $40\%/\sqrt{100} = 4\%$ determination of the gain and 10% determination of relative QE *per tube*, which leads to a (detector averaged) precision of $4\%/\sqrt{200} = 0.3\%$ and $10\%/\sqrt{200} = 0.7\%$ on the PMT gain and relative QE. Assuming a 100 Hz photoelectron rate in a detector module, this step of the calibration can be performed in 5 minutes.

3.2 Scintillation Yields and Attenuation Lengths in the Target and Gamma Catcher

Aside from some detector defects (e.g. dirty acrylic), the property of a detector can be largely parameterized by the scintillation light yield, attenuation length, as well as the reflectivity of the inner wall. We shall first discuss the calibration of the former two. The reflectivity causes “late light arrival” (details of the timing spectrum will be shown in Sec. 3.4). We eliminated its effect from this step by requiring a timing cut: hits within 5 ns after the expected t_0 calculated from the line-of-sight. The effect of the attenuation of acrylic vessels are tiny (Table 1), and is neglected as well.

As illustrated by Fig. 1, in our 3-zone detector, both the light yields in the target and gamma catcher need to be determined accurately. To first order, assuming that a calibration source deposits energy only locally, the total detector yields for source in the two regions directly reflect the light yields in them. The attenuation length, on the other hand, causes the response of a phototube to vary with vertex position *beyond the acceptance effect*. Therefore, by deploying a source at different locations in the detector module, and by analyzing the total light yield as well as the PMT hit pattern, it is conceivable that one can separate out all these parameters.

To study the feasibility of this plan, we simulated a calibration program as illustrated in Fig. 2. A 1 MeV electron source [†] was deployed along z axis ($z = 1.835, 1.4, 1.0, 0.5, 0, -0.5, -1.0, -1.4$ m) at three r locations: $x = 0$ (center), 1.4 (edge), and 1.835 m (gamma catcher). At each given location, 100 source events were generated. To get the detector parameters, we constructed a likelihood function as follows. Let $N_{n,i}$ be the measured PE of tube i in event n , corresponding to a Poisson probability of

$$P_{n,i} = \frac{(\mu_{n,i})^{N_{n,i}} e^{-\mu_{n,i}}}{N_{n,i}!}. \quad (1)$$

In this expression μ_i is the expected number of PEs in tube i , which is a function of vertex position in event n (\vec{x}_n), light yields Y_{tgt} and Y_{gcat} , and attenuation lengths L_{tgt} , L_{gcat} , and L_{mo} :

$$\mu_{n,i} = \text{QE} \times E_{\text{src}} Y_{\text{light}} \frac{\Omega_i(\vec{x}_n)}{4\pi} e^{-\left(\frac{d_{\text{tgt}}}{L_{\text{tgt}}} + \frac{d_{\text{gcat}}}{L_{\text{gcat}}} + \frac{d_{\text{mo}}}{L_{\text{mo}}}\right)}, \quad (2)$$

[†]For simplicity we used an electron source instead of a gamma source so that the ionization energy is deposited locally.

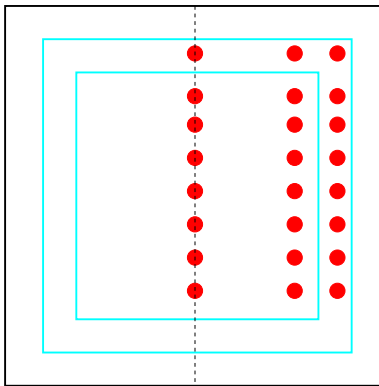


Figure 2: *Illustration of the source deployment plan.*

where QE is an average quantum efficiency of the tube, which we fixed at 0.2. d_{tgt} , d_{gcat} , and d_{mo} are the distances the light travels in the target, gamma catcher, and mineral oil, respectively. Y_{light} takes the value of Y_{tgt} or Y_{gcat} depending on the source position. It is noteworthy that the actual photons produced by GEANT4 is not simply $Y_{\text{light}} \times E_{\text{src}}$; it also depends on the delta-ray production threshold [3]. This (scaling) effect is absorbed into the fitted values of Y_{tgt} and Y_{gcat} . Therefore one should take the ratio of the fitted Y_{tgt} and Y_{gcat} , instead of their values, to validate the fit. The overall likelihood function is the product of the Poisson probabilities for individual events and tubes:

$$\mathcal{L} = \prod_{n,i} P_{n,i}. \quad (3)$$

The best estimators of parameters are obtained by maximizing \mathcal{L} , or equivalently minimizing $-\text{Log}(\mathcal{L})$.

In the Monte Carlo, we made several variations to the parameters, and used the likelihood function above to fit for the parameters. The fitted attenuation length for the mineral oil was not stable, possibly due to relatively short distance that the light travels in it. Therefore we simply fixed L_{mo} at the nominal value (13 m). In some cases we also fixed L_{gcat} in order to obtain better fit to other parameters. A comparison of the inputs and the fits are made in Table 2. The statistical uncertainty of the fitted light yields are typically 1%, and that of the attenuation length is <0.3 m. Apparently the fitting procedure is sensitive to large change of the parameters, and is able to tell a large change of light yield from a large change of attenuation. This is very encouraging given this is our very first attempt of this method. Among all, the accuracy of the fit to L_{tgt} is more-or-less satisfactory, particularly when the attenuation gets worse. On the other hand, the difference of $Y_{\text{tgt}}/Y_{\text{gcat}}$ and L_{gcat} to their true values are roughly a factor of 2 to 3 to the specs. It appears that the fit tends to under-predict the value of $Y_{\text{tgt}}/Y_{\text{gcat}}$ (in some cases as large as 5%!) and L_{gcat} (by 20%). In any case, this simple exercise demonstrates that a program as shown in Fig. 2 is sensitive to a large set of parameters. The precision of the procedure is likely improve to the desired level as more simulation studies are carried out.

3.3 Attenuation in the Mineral Oil

The measurement of the attenuation in the mineral oil will be more straightforward if one can put light source directly in the oil buffer. Fig. 3 shows one such possibility: one LED diffuser ball is located in the vertical oil buffer (offset from the center plane), and a phototube is implemented at the top (bottom) of the steel tank looking down (up). Ideally, the ratio of the rates measured in the two tubes, corrected for the differing acceptance, leads directly to the attenuation length. Realistically, non-negligible difference might exist in the sensitive areas and efficiencies between the two tubes. One can put another LED ball at a different z location, then the ratio of the two ratio measurement will be insensitive to such systematics. Possible contaminations from the reflection can be removed by requiring a tight timing cut.

To study the feasibility of this system, we implemented two (identical) top and bottom tubes into *G4dyb*, and generated optical photons isotropically. The input attenuation length of the mineral oil L_{mo} was varied from run to run, and measured by taking the ratio of the acceptance-corrected rates seen in the two

Parameter Set	Input Value	Fitted Values
$Y_{\text{tgt}}/Y_{\text{gcat}}$	1.0	0.955
L_{tgt} (m)	9.0	9.99
L_{gcat} (m)	10.0	fixed at 10.0
$Y_{\text{tgt}}/Y_{\text{gcat}}$	0.667	0.674
L_{tgt} (m)	9.0	9.32
L_{gcat} (m)	10.0	fixed at 10.0
$Y_{\text{tgt}}/Y_{\text{gcat}}$	0.75	0.743
L_{tgt} (m)	9.0	9.95
L_{gcat} (m)	10.0	fixed at 10.0
$Y_{\text{tgt}}/Y_{\text{gcat}}$	1.0	0.978
L_{tgt} (m)	4.5	4.6
L_{gcat} (m)	10.0	fixed at 10.0
$Y_{\text{tgt}}/Y_{\text{gcat}}$	1.0	0.977
L_{tgt} (m)	9.0	8.2
L_{gcat} (m)	5.0	4.2
$Y_{\text{tgt}}/Y_{\text{gcat}}$	1.0	0.947
L_{tgt} (m)	4.5	4.6
L_{gcat} (m)	5.0	4.0
$Y_{\text{tgt}}/Y_{\text{gcat}}$	1.333	1.275
L_{tgt} (m)	4.5	4.6
L_{gcat} (m)	10.0	fixed at 10.0
$Y_{\text{tgt}}/Y_{\text{gcat}}$	1.333	1.252
L_{tgt} (m)	4.5	4.55
L_{gcat} (m)	5.0	4.0

Table 2: A comparison of the input and fitted values of various sets of parameters in the likelihood fitter.

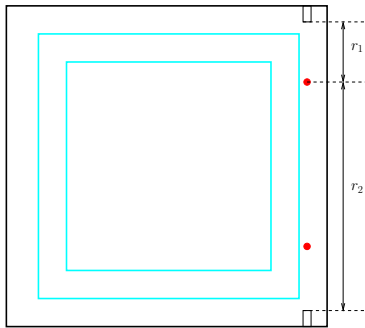


Figure 3: Illustration of a LED system in the mineral oil to calibrate the attenuation length of the oil.

phototubes. The comparison between the fitted and true values of L_{mo} is made in Fig. 4. Within (limited) statistics, the measured and the true L_{mo} agree. When the true value of L_{mo} is 13 m, the measured value is 14.9 ± 4.7 . It is perhaps fair to say that we are within a factor of two of the specs in Table 1. Further MC studies are underway.

3.4 Reflectivity

The diffusive reflectivity of the steel tank is difficult to calibrate accurately. The nominal reflectivity (0.1) increases the total PE yield by less 10%, and they are difficult to be identified in the timing spectra. For now, we advocate to make the vertical wall completely black to eliminate the ambiguity in both calibration and reconstruction. On the other hand, the top and bottom aluminum reflector will have unique signature

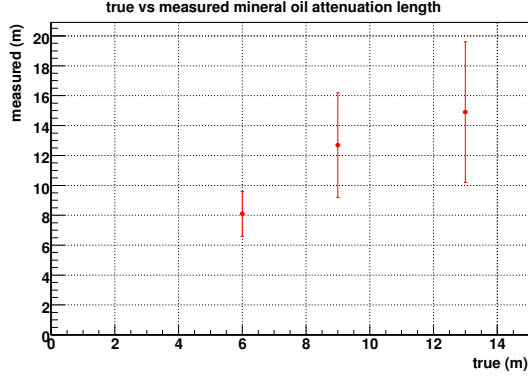


Figure 4: Comparison between the true and measured attenuation lengths of the mineral oil. Each data point corresponds to roughly 1000 hits in the “far tube”.

in the data, due to their high specular reflectivity. In Fig. 5, the timing spectrum for ring 2 (2nd ring of PMTs from the bottom) are plotted for a source located at the center. The spectra without top or bottom reflector are overlaid. One sees that for a detector with both reflectors (black histogram), the main peak

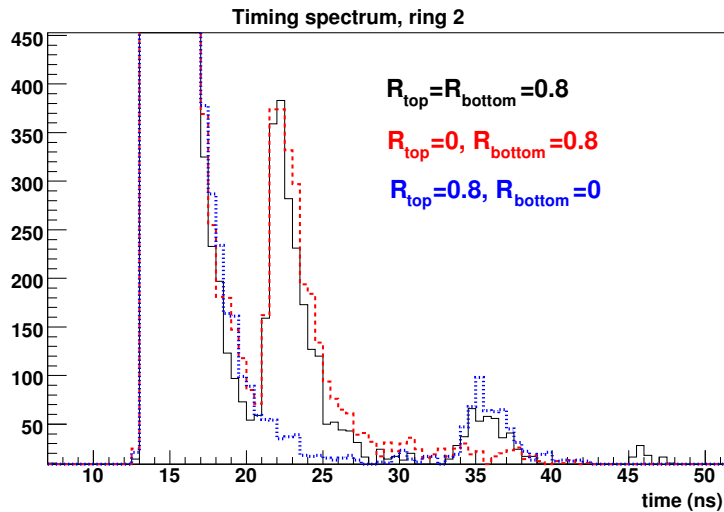


Figure 5: Timing spectra for ring 2 (2nd ring from the bottom) when the source is deployed at the center. Black: $R_{top} = R_{bottom} = 0.8$; red: $R_{top} = 0, R_{bottom} = 0.8$; blue: $R_{top} = 0.8, R_{bottom} = 0$.

(with the top being cut off) corresponds to direct hits, and the 2nd and third peaks are due to either one of the reflectors. In principle, by applying the timing cut and taking the ratio of the direct and reflected peaks, combined with the attenuation and acceptance, one could extract the reflectivity. It is also conceivable that by adding a reflection term in Eqn. 2 [6], one can determine the reflectivity via likelihood fit when performing the source z scan. However, the timing uncertainty due to the scintillation light delay might prevent a clear separation of the direct and reflected events. Furthermore, the ratio of the bottom reflected peak to the direct peak in Fig. 5 can not easily distinguish a degraded bottom reflector from a dirty acrylic.

Alternatively, one could design a direct way to measure the reflectivity. Fig. 6 shows an example in which an isotropic light source (such as an LED source) is planted at the bottom buffer region. A collimated photo-sensor, of which the orientation can be controlled remotely, is also implemented in the oil buffer. One runs the sensor at two orientations: one views directly the source, and the other views the reflection. As shown in the figure, since the distances that the direct and reflected lights travel in the mineral oil are not too different, the ratio of the two types of rates the photo-sensor sees (corrected for acceptance) gives the reflectivity. We

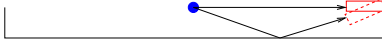


Figure 6: A diagram for a system that measures the reflectivity of the aluminum reflectors.

validate this concept with a (perhaps over-simplified) simulation using *G4dyb*. A phototube is implemented at the position of the sensor in Fig. 6, and optical photons are generated with perfect directions, either going straight or getting reflected into the tube. R_{bottom} was varied from 0.8 to 0.2, and its extracted value is plotted in Fig. 7. One sees that at least in principle, the top/bottom reflectivity can be measured to the desired precision with such a simple device.



Figure 7: True vs. measured reflectivity from the *G4dyb* simulation.

3.5 Dirt at the Bottom of the Inner and Outer Acrylic Vessel

In [4], we have made the “dirt” very opaque ($L_{dirt}^{in} = L_{dirt}^{out} = 1$ cm) and shown that it causes a strong dependence of the signal vs. z , which can be detected by a source z scan (Fig 8(a)). For comparison, the same z scan was made on a detector with a degraded bottom reflector ($R_{bottom}=0.2$). The results are plotted in Fig. 8(b), from which one observes a less strong z dependence. However, it was pointed out at the Berkeley review that in reality, a “not-so-opaque” acrylic might still be confused with a bad reflector from the z scan. As mentioned earlier in Sec. 3.4, the late light information from the timing spectra can not distinguish the

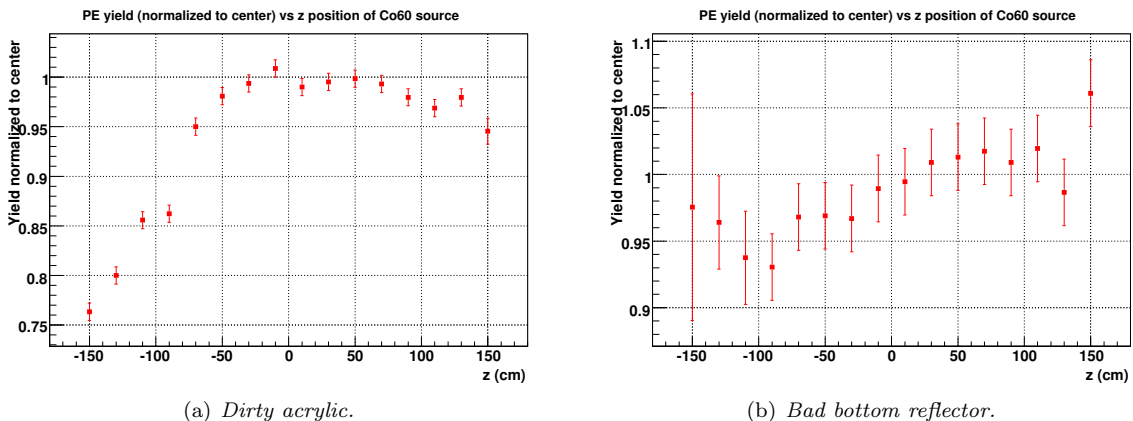


Figure 8: The results of a scan of ^{60}Co source along the central z axis for a detector with a) dirty acrylic with $L_{dirt}^{in} = L_{dirt}^{out} = 1$ cm, and b) bad bottom reflector with $R_{bottom}=0.2$.

two effects either. Thus, we shall aim to measure L_{dirt}^{in} and L_{dirt}^{out} directly.

A possible system for such a purpose is sketched in Fig. 9. Three LED diffuser balls are “planted” at the

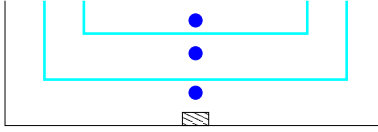


Figure 9: A diagram for a system that monitors the optical properties of the bottom of two acrylic vessels.

bottom of the detector, one in each zone. One PMT facing up is implemented at the bottom of the steel tank. In reality the tube will probably need to be offset from the axis defined by the three sources to avoid any obstruction of the acceptance. However one should make sure that it views the sources at small angles so that the internal reflections from the acrylic is not an issue. Once again, we ran an oversimplified *Geant4* simulation by throwing optical photons straightly to the tube (so we can ignore the acceptance effect) at the three source locations. The input values for $L_{\text{dirt}}^{\text{in}}$ and $L_{\text{dirt}}^{\text{out}}$ were varied. The measured counts in the bottom tube in each case were first corrected for the attenuation effects from the liquids, after which $L_{\text{dirt}}^{\text{in}}$ and $L_{\text{dirt}}^{\text{out}}$ can be extracted from ratios of rates. A comparison of the values of the “true” and “measured” $L_{\text{dirt}}^{\text{in}}$ and $L_{\text{dirt}}^{\text{out}}$ are made in Table 3. Although the method seems to systematically favor a slightly shorter attenuation length, the agreement between the true and predicted values are within the specs in Table 1. The bottom line is that if the acrylic become somewhat dirty in the real experiment, this implementation will detect and allow a quantitative measurement of the degradation.

Parameter	Input Value	Extracted Value
$L_{\text{dirt}}^{\text{in}}$ (cm)	10	9.0(0.8)
$L_{\text{dirt}}^{\text{out}}$ (cm)	10	8.0(0.7)
$L_{\text{dirt}}^{\text{in}}$ (cm)	20	14.3(2.0)
$L_{\text{dirt}}^{\text{out}}$ (cm)	10	9.0(0.8)
$L_{\text{dirt}}^{\text{in}}$ (cm)	5	4.5(0.2)
$L_{\text{dirt}}^{\text{out}}$ (cm)	50	32(9)

Table 3: Comparison of the input and extracted values for $L_{\text{dirt}}^{\text{in}}$ and $L_{\text{dirt}}^{\text{out}}$.

3.6 Spallation Neutron

Besides the direct calibration devices we have discussed, the spallation neutron events serve as a unique and powerful calibration tool. The 2.2 MeV n-p and 8 MeV n-Gd capture signals are distributed uniformly throughout the detector. Combined with the vertex reconstruction, one can produce a full volume map of the detector response, as shown in Fig. 10. Effectively, the topology of this map captures the combined effect of all detector parameters. We have shown in [1] that even without detailed knowledge of individual parameters, we can use the spallation neutron capture peak to set the overall energy scale and achieve near/far “identical” neutron efficiency. In what follows, we shall outline an alternative (and perhaps less aggressive) plan in using the spallation neutrons, in response to the Berkeley review comments. We assume that the standard source/LED program is carried out and has measured individual detector parameters. We also assume that these parameters enter as inputs to the energy reconstruction (see Sec. 4).

- The reconstructed spallation neutron capture events close to the three calibration axes should agree with the direct neutron source calibration along them. This is the first validation of the program.
- The n-p capture signals in the gamma catcher can provide further information about the detector properties there. This is particularly useful at the bottom of the gamma catcher, where direct calibration device has no access.
- The reconstructed n-p capture peak should be at 2.2 MeV, and that of n-Gd capture should be at 8 MeV, *regardless of the vertex position*. If position non-uniformity is found, it either indicates that

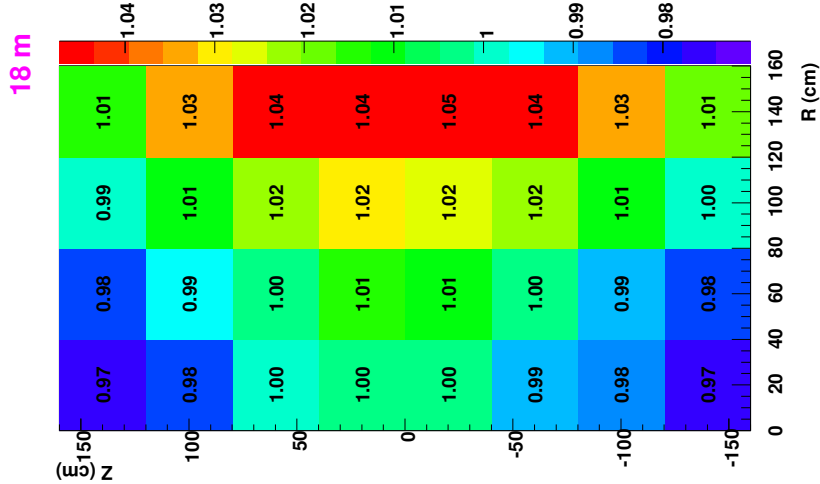


Figure 10: *The Gd capture PE yield for the spallation neutrons (normalized to the yield at the detector center) as a function of the neutron vertex (R, z). Picture rotated by 90° .*

some parameters in the model are off, or that our detector modeling is imperfect. One should try best to diagnose and fix the problem, in effect, turning Fig. 10 into a flat energy map.

- It is conceivable that after exhausting all techniques, some residual non-uniformity in the neutron energy map remains. Then one could consider taking the residual map to make the final position dependent energy correction.

The effectiveness of the 2nd bullet requires further Monte Carlo studies.

4 Energy Reconstruction

In this section, we shall discuss the general methodology of reconstructing event energy. In contrast to the simple method in [1], we shall apply the detector parameters obtained in Sec. 3, combined with the measured charge, hit pattern, and perhaps timing information, to make *vertex dependent* energy reconstruction.

The principle of such a reconstruction relies on an event-by-event likelihood fit to the visible energy estimator. According to the discussion in Sec. 3.2, in a given event n we construct the likelihood function[§] as

$$\mathcal{L}_n = \prod_i P_{n,i}, \quad (4)$$

in which $P_{n,i}$ is the Poisson probability for tube i in this event (Eqn. 1). The key action in this practice is to properly model the expected hits in tube i , $\mu_{n,i}$, which will be a function of the event energy, position, and detector parameters. Eqn. 2 gives a naive starting point of such a model, and we envision that it will become more sophisticated to reflect reality. In any event, the reconstruction is an opposite process to the calibration: one takes the calibrated parameters and fit for the event energy.

A few critical questions in the reconstruction remain to be addressed by the simulation. First, in principle the likelihood fit is able to determine the vertex position and energy simultaneously. Alternatively, one can first determine the vertex position, then fit for the energy. Which method is more robust? Second, if we choose the latter method, what is the best way to reconstruct position? Perhaps the simplest method is to use the source data (Fig. 2) to calibrate an empirical correction to the charge center. A more sophisticated method is to use the PMT hit pattern and timing as described in [5]. Preliminary study indicates that the

[§]We use the symbol \mathcal{L}_n with the subscript n labeling an event to emphasize that the maximum likelihood fit is made for each individual event. For source calibration procedure in Sec. 3, we multiplied \mathcal{L}_n for all events into a “grand” likelihood function and then fit to get the parameters, since all events share the same energy.

latter method can get to <20 cm resolution, which is much more precise than using the “calibrated” charge center (Fig. 11), but slightly worse than the resolution from the energy and position vertex combined fit (14 cm) [2]. Further studies are needed to take into account the scintillation timing delay and electronics jit-

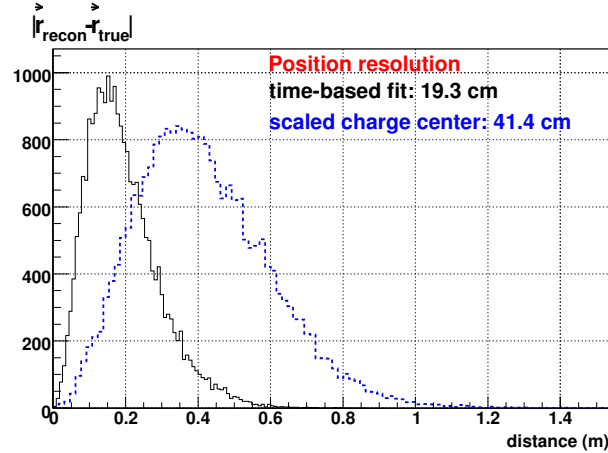


Figure 11: *Position resolution (the distance between the true and reconstructed vertices) for the time-based method (black solid) and “corrected charge center” method (blue dashed).*

ter, etc. The systematic effect of the reflected lights in the second method also needs to be addressed. Third, what is the best approach to treat reflected light in both the calibration fit and the energy reconstruction? In particular, can we make efficient use the “late light” information as shown in Fig. 5? Alternatively, is it practical to add a term for reflected lights (see [6]) in Eqn. 2.

In summary, we have modified our reconstruction plan: that the event energy will be determined from a (position dependent) likelihood fit using the calibrated parameters. The spallation neutron signals will be the validation of the procedure, as well as providing the final “ad hoc” correction.

5 Summary and Outlook

We have presented a modified detector calibration plan, in response to the charges received at the Berkeley review. Some very preliminary studies of the feasibility have been discussed in this note. We believe a calibration program with radiative/LED sources along three z axes, with some additional diagnostic devices, in combination with the spallation neutrons, will allow us to calibrate the detector to desired precision.

The proposed calibration devices in this note are only conceptual. In the near future, various technical designs will emerge, and we are considering the possibility of integrating the radioactive sources and the LED system. The simulation work at the next stage will be focused on three aspects: a) refining the calibration likelihood fitter, b) implementing realistic radioactive source geometry, and c) working towards an efficient and robust event reconstruction.

References

- [1] J. Liu, et. al., Some Simulations of the Daya Bay Calibration System, Daya Bay DocDB-333
- [2] Daya Bay Physics Proposal.
- [3] J. Cao, G4dyb Discussions, Daya Bay DocDB-384.
- [4] J. Liu, Simple Simulation of Dirt at the Acrylic Bottom, Daya Bay DocDB-400.
- [5] Jason Detwiler Ph.D. thesis (Sec. 4.3.2), Stanford University, 2005.
- [6] J. Cao, Simulation and Reconstruction Summary, Daya Bay DocDB-87.